RSC Advances

This is an *Accepted Manuscript*, which has been through the Royal Society of Chemistry peer review process and has been accepted for publication.

Accepted Manuscripts are published online shortly after acceptance, before technical editing, formatting and proof reading. Using this free service, authors can make their results available to the community, in citable form, before we publish the edited article. This *Accepted Manuscript* will be replaced by the edited, formatted and paginated article as soon as this is available.

You can find more information about *Accepted Manuscripts* in the Information for Authors.

Please note that technical editing may introduce minor changes to the text and/or graphics, which may alter content. The journal's standard Terms & Conditions and the Ethical guidelines still apply. In no event shall the Royal Society of Chemistry be held responsible for any errors or omissions in this *Accepted Manuscript* or any consequences arising from the use of any information it contains.

ROYAL SOCIETY OF CHEMISTRY

www.rsc.org/advances

A label-free fluorescent probe for Hg^{2+} based on boron- and nitrogen-doped photoluminescent WS_2

Xiaojia Liu, Yizhi Zheng, Qian Xiao, Na Wu, Suiping Wang*, Bo Feng*

College of Chemical Engineering, Xiangtan University, Xiangtan 411105, Hunan Province, China

*Corresponding Authors. Tel.: +86 731 58298259; Fax: +86 731 58298172.

E-mail address: fengbo@xtu.edu.cn; fengbo5460@hotmail.com

RSC Advances Accepted Manuscript

ABSTRACT

The air-stable doping of transition-metal dichalcogenides is important in enabling a wide range of optoelectronic and electronic devices while exploring basic material properties. In this work, we develop for the first time a simple, low-cost synthesis route to preparing boron-and-nitrogen-doped WS_2 (B,N-WS_2) nanosheets. Bulk WS_2, a prototypical transition-metal chalcogenide material, is an indirect band-gap semiconductor with negligible photoluminescence. The obtained B,N-WS_2 nanosheets exhibited enhanced fluorescence. The B,N-WS_2 nanosheets can be used as a green and easy sensing platform for the label-free detection of Hg^{2+} because of the high sensitivity and selectivity toward Hg^{2+}. Detection can also be easily accomplished through a rapid, one-step (within 1 min) operation, with a limit as low as 23 nM ($S/N = 3$).

Keywords**:** B,N-WS_2; fluorescence; sensor; Hg ion

RSC Advances Accepted Manuscript

1. Introduction

Heavy metal ion pollution has become a critical worldwide issue for years because of severe risks to human health and the environment[1]. Mercury ion has been recognized as one of the most toxic transition-metal ions in the world by the United States Environment Protection Agency[2]. Hg^{2+} has been demonstrated to be able to easily pass through skin, respiratory, and gastrointestinal tissues into the human body and damage the central nervous and endocrine systems[3], thereby raising serious environmental and health concerns. These health and environmental problems of the mercury (II) ion have prompted the development of efficient, rapid, facile, and applicable methods for the sensitive and selective assay of mercury (II) ion. Therefore, a convenient and rapid method for the analysis of Hg^{2+} ions is highly desirable. Fluorescence-based mercury (II)-ion detection has attracted considerable interest because of its simple operation, high sensitivity, and adaptability for in-field measurement. Recently, numerous studies have been reported for the detection of these ions[4–8]. So far, a wide variety of fluorescent probes have been developed, including fluorescent dyes organic molecules, noble metal nanoclusters and metal-based quantum dots (MQDs) etc. Zhang et al.[9] described a novel Rhodamine-Based Fluorescent Chemosensor as an “off-on” fluorescent probe for the detection of Hg^{2+} in aqueous samples. Lin et al.[10] demonstrated the use of lysozyme type VI-stabilized gold nanoclusters (LysVI-AuNCs) for the detection of Hg^{2+} based on fluorescence quenching. Zhou et al.[11] developed carbon nanodots as fluorescence probes for rapid, sensitive, and label-free detection of Hg^{2+}. Such fluorescent probes,

RSC Advances Accepted Manuscript

however, suffer from photobleaching of fluorescent dye, expensive cost of noble metals, or toxicity of MQDs, limiting their widespread applications.

Over the past two decades, two-dimensional (2D) transition-metal dichalcogenides (TMDs) have garnered considerable attention from scientists, leading to wide-ranging and diversified technological applications because of their unusual properties[12–15]. TMDs are MX_2 type compounds, where M is a transition metal belonging to groups IV, V, and VI, and X is a chalcogen, such as S, Se, and Te[16–18]. For bulk-layered TMDs, strong intralayer covalent M-X bonds exist, while weak van der Waals interactions connect the adjacent layers, which could be cleaved to few-layer nanosheets. The properties of 2D TMDs are found to be advantageous in other branches of science, such as biosensors and nanomedicine, taking advantage of large surface area, good biocompatibility, fluorescence, electrical conductivity, and rapid heterogeneous electron transfer[19,20]. TMDs, typically MoS_2 and WS_2, are the most important grapheme-like two-dimensional layered materials. WS_2 has been the subject of substantial interest because the band gap is well matched to the solar spectrum[21]. WS_2 can act as an efficient photoconductive layer in photovoltaic devices and photoelectrochemical solar cells[22.] The main advantage of WS_2 is corrosion prevention, as phototransitions involve nonbonding *d–d* orbitals of W atoms[23]. WS_2 is a quasi-two-dimensional compound, with covalently bonded S–metal–S sheets held by van der waals forces. In addition, the unique combinations of structural, electronic, catalytic, mechanical, and related properties of the material can offer superiority in applications of biosensors and nanomedicine for achieving detection, diagnosis, and

RSC Advances Accepted Manuscript

therapy with high sensitivity, specificity, and accuracy. Heteroatom doping can drastically alter the electronic characteristics of TMDs, thus resulting in unusual properties and related applications. Ultra-thin, ultra-small, defect, and doped WS_2 prepared by different researchers have shown excellent applications in semiconductors and fluorescence materials[24,25].

For the first time in this study, we report a facile and low-cost synthetic strategy to prepare fluorescent nanosheets of B,N-WS_2 by doping WS_2 with boron and nitride using the doping method to change the band gap of WS_2. Boron and nitrogen atoms were incorporated in WS_2 by co-annealing with boric acid and melamine. The as-prepared samples were demonstrated as a highly effective fluorescent-sensing platform for label-free, sensitive, and effective Hg^{2+} detection with a detection limit of as low as 23 nM. The entire detection process can be completed within 1 min. The proposed design is simple to prepare and exhibits low background interference, high sensitivity, and ultrafast response. This work successfully demonstrates that the introduction of boron and nitrogen elements into ultrathin WS_2 nanosheets for enhanced fluorescence properties is feasible through a facile and general preparation strategy. This study may open up a potential approach toward designing more efficient TMD-based biosensors and fluorescence material.

2. Experimental section

2.1 Materials

$Hg(Ac)_2$, $Fe(NO_3)_2$, $Fe(NO_3)_3$, $Cu(NO_3)_2$, $CaCl_2$, $LiNO_3$, $NaNO_3$, KNO_3, $Zn(Ac)_2$, $Mg(NO_3)_2$, $Ni(NO_3)_2$, $Pb(NO_3)_2$, $Mn(NO_3)_2$, $Ba(NO_3)_2$, and $CoCl_2$ were purchased

RSC Advances Accepted Manuscript

from Aladdin Ltd. (Shanghai, China). All reagents are of analytical grade and were used as received without further purification. Double-distilled water was used throughout the experiments.

2.2 Characterizations

Fluorescent emission spectra were recorded on a F-7000 spectrofluorometer (Hitachi, Japan). Ultraviolet–visible (UV–vis) spectra were recorded with a UV-1800 spectrophotometer (Shimadzu, Japan). The morphology of products was investigated by scanning electron microscopy (SEM, Hitachi S-4800, Japan) at 5.0 kV accelerating voltage. X-ray diffraction (XRD) analysis was carried out on a BRUKER D8-ADVANCE X-ray diffractometer by using Cu (40 kV, 40 mA) radiation. Raman spectra were obtained using a laser confocal Raman spectrometer (LABRAM-010) in the range of 300 cm^{-1} to 2000 cm^{-1}. Transmission electron microscopy (TEM) images were obtained using a JEM-3010 (JEOL-3010, Japan). Metrology X-ray photoelectron spectroscopy (XPS) was carried out using Kα 1063 type with focused monochromatized Al Kα radiation (1486.6 eV).

2.3 Synthesis of B,N-WS_2

In a typical synthesis, bulk WS_2 (0.5 g) was thoroughly mixed with a solution of boric acid (1 g) and melamine (1 g) in anhydrous ethanol (100 mL) by ultrasonic dispersion for 1 h. The mixture was dried at 80 °C, subsequently heated to 400 °C in N_2 atmosphere at a heating rate of 5 °C min^{-1}, and maintained for 2 h. The sample was cooled to room temperature to obtain the B,N-WS_2 powder. In a typical run, 10 mg of B,N-WS_2 powder was added to 100 mL of deionized water. After ultrasonic

RSC Advances Accepted Manuscript

dispersion for 2 h, the precipitate was removed by centrifugation at 2000 rpm for 3 min, and the clear supernatant extract was prepared for analysis.

2.4 Detection of Hg ions

Hg ions were detected at room temperature in aqueous solution. Hg aqueous solutions at different concentrations, together with other metal ion solutions, were freshly prepared before use. To evaluate the sensitivity towards Hg^{2+}, we added different concentrations of Hg^{2+} into the as-prepared supernatant of B,N-WS_2. The mixed solutions were equilibrated for 2 min before spectral measurements. Photoluminescence (PL) spectra were recorded by operating a fluorescence spectrophotometer at 280 nm excitation wavelength.

3. Results and discussion

3.1 Characterizations of B,N-WS_2

The morphologies of the as-prepared B,N-WS_2 were characterized by SEM and TEM. Figs. 1 (a) and 1 (b) display the SEM image of bulk WS_2. The SEM image indicates that bulk WS_2 is solidly agglomerated at approximately several micrometers in size and exhibit the accumulation of large structures. Meanwhile B,N-WS_2 did not retain the original morphology of bulk WS_2 after the doping process. In contrast, a thin-layer structure is shown in Figs. 1 (c) and 1 (d), demonstrating that boron- and nitrogen-doped WS_2 two-dimensional layered ultrathin nanosheets have been successfully prepared after doping and ultrasonication.

RSC Advances Accepted Manuscript

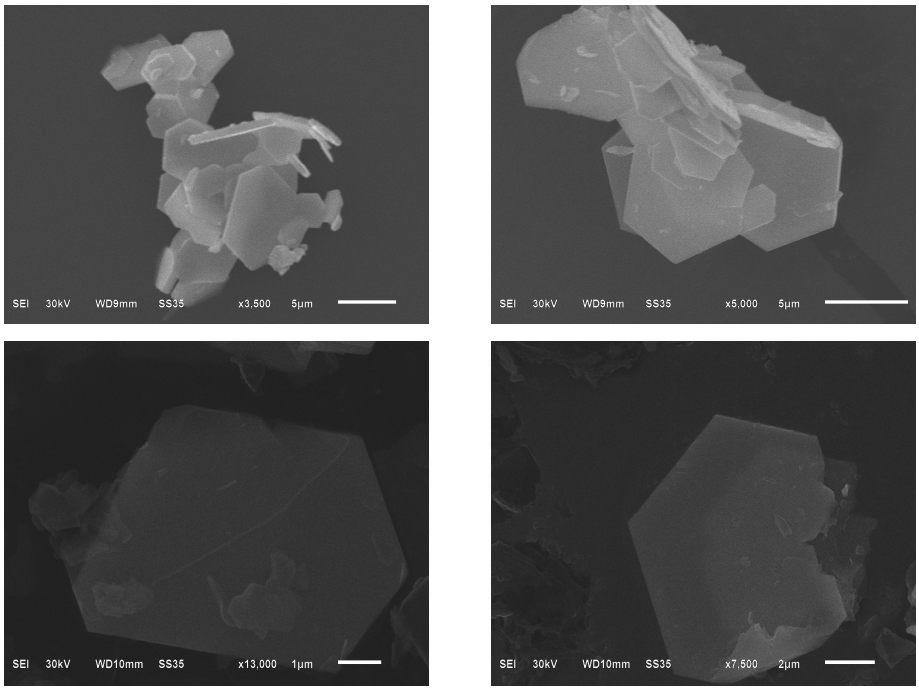

Fig. 1 SEM images of bulk WS_2 (a) (b) and B,N-WS_2 (c) (d).

TEM was carried out to further analyze the layer structure of B,N-WS_2. Fig. 2 (a) shows the image of B,N-WS_2, which possesses a layer structure at the micrometer scale. Ultrathin structure can be seen clearly in Figs. 2 (b) and 2 (c). The inset of Fig. 2 (d) shows the high resolution transmission electron microscopy (HRTEM) image of B,N-MoS_2, with the (002) crystal plane spacing of 0.62 nm of the lattice. The result fits well with the XRD result. Fig. 2 indicates that the layered nanosheets are successfully prepared.

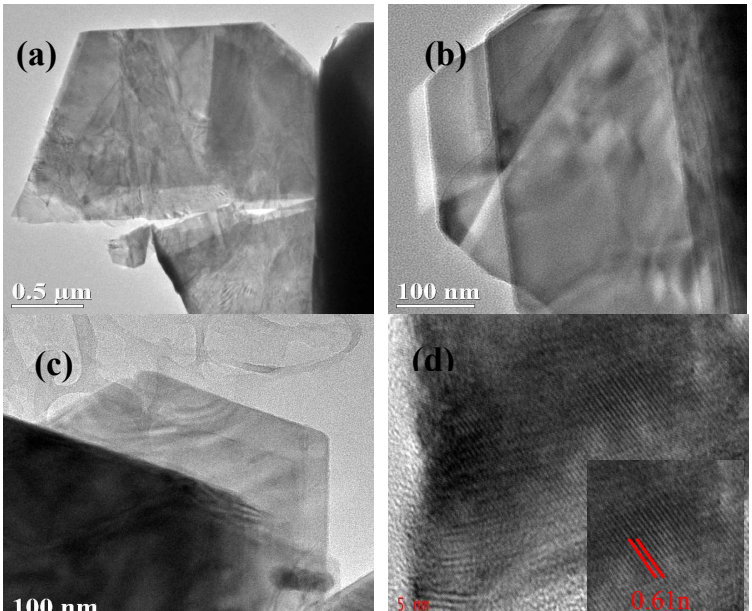

RSC Advances Accepted Manuscript

Fig. 2 TEM (a) (b) and (c) and HRTEM (d) analysis of B,N-WS_2.

In addition, the crystalline structure of bulk WS_2 and B,N-WS_2 were determined by powder XRD (Fig. 3). The peaks at 14.3°, 28.9°, 32.7°, 33.5°, 39.5°, 44.0°, 58.4°, 59.9°, and 60.4° correspond to the (002), (004), (100), (101), (103), (006), (105) (110), and (112) reflections of bulk WS_2 (indexed by Chem. Mater., Vol. 12, No. 5, 2000), respectively. For B,N-WS_2, the peaks at 14.4°, 28.9°, 32.8°, 33.5°, 39.7°, 44.0°, 58.3°, 59.8°, and 60.5°correspond to the (002), (004), (100), (101), (103), (006), (105), (110), and (112) reflections, respectively. Compared with bulk WS_2, the *d* spacing of B,N-WS_2 decreases from 0.61372 nm to 0.61213 nm, indicating that B and N were doped into the WS_2 structure.

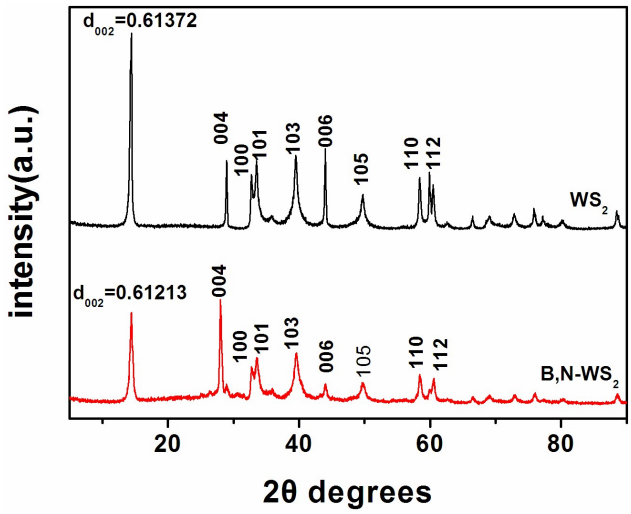

Fig. 3 XRD pattern of bulk WS_2 and B,N-WS_2

XPS was conducted to analyze the chemical states of W and S in the bulk WS_2 and B,N-WS_2 samples (Fig. 4). According to the full survey spectra in Fig. 4 (a), the elements W, S, C, and O are found in all samples. However, B and N are found on the

RSC Advances Accepted Manuscript

B,N-WS_2 sample, indicating that B and N were successfully doped into WS_2. The W 4*f* doublet peak energies 32.75 eV (W $4f_{7/2}$) and 34.9 eV (W $4f_{5/2}$), and S 2*p* double peak energies 162.55 (S $2p_{3/2}$) and 163.8 eV (S $2p_{1/2}$) are identified in the spectra. The binding energies are in good agreement with the reported values for WS_2 samples[19]. The peaks corresponding to the S $2p_{3/2}$ and S $2p_{1/2}$ similar to the bulk WS_2 sample. However, compared with the bulk WS_2 sample, the XPS spectrum of B,N-WS_2 shows W 4*f* peaks are shifting toward higher binding energies at 33.35 and 35.8 eV, indicating that boron and nitrogen elements are successfully doped into WS_2. These results agree with the EDS result of the B,N-WS_2 sample (Supporting Information, Fig. S1).

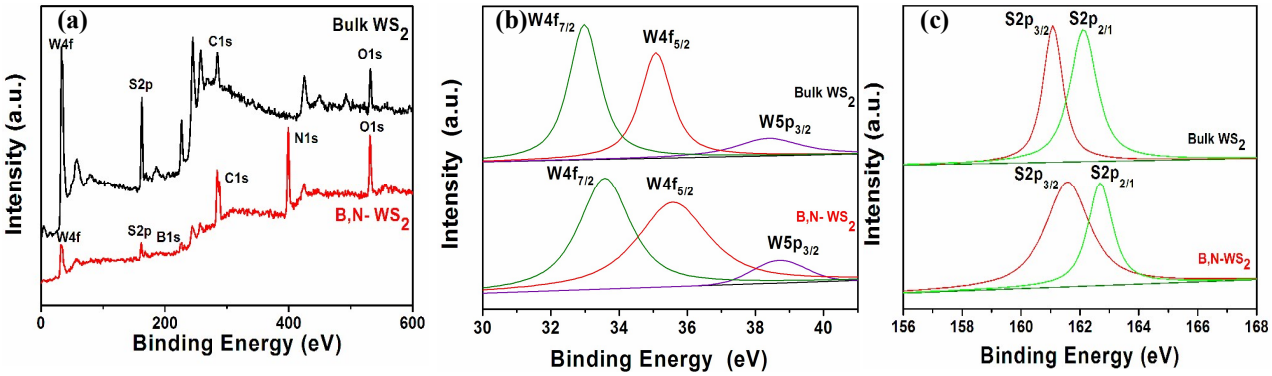

Fig. 4 XPS spectra of bulk WS_2 and B,N-WS_2.

Fig. 5 (a) shows the PL emission spectra of B,N-WS_2 and bulk WS_2 at the same concentration and excitation at 280 nm. Notably, the fluorescence of the bulk WS_2 dispersion can almost be ignored. However, the B,N-WS_2 dispersion shows a strong PL emission peak centered at 343 nm, indicating that the nanosheets are fluorescent. Fig. 5 (b) shows the UV-vis absorption and PL emission spectra of B,N-WS_2 dispersion in water. The UV-vis spectrum shows an absorption peak at 220 nm. The

RSC Advances Accepted Manuscript

dispersion exhibits a strong PL emission peak centered at 343 nm when excited at 280 nm, indicating that the B,N-WS_2 nanosheet exhibits strong fluorescence.

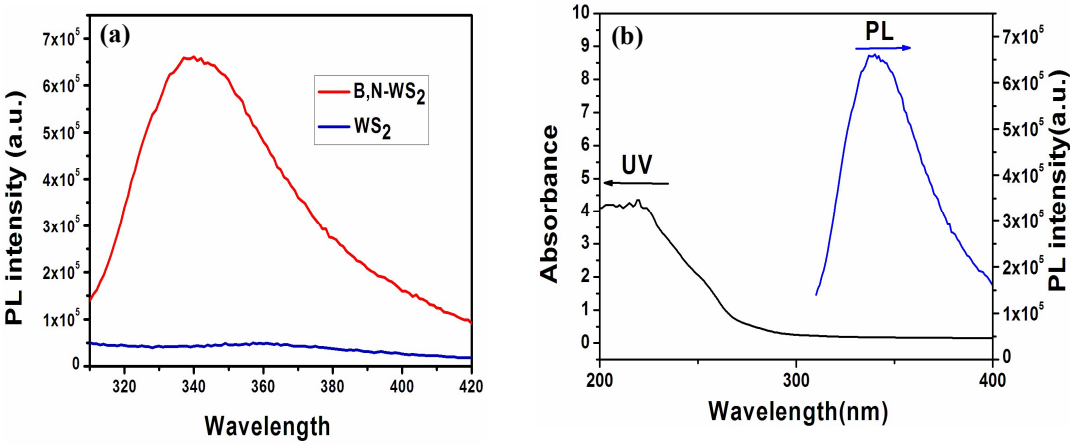

Fig. 5 PL spectra of B,N-WS_2 and bulk WS_2 (λ_{ex} = 280 nm) (a); UV, and PL spectra of B,N-WS_2 (b).

The luminescence quantum yield and emission lifetime of B,N-WS_2 have been estimated. Fluorescence quantum yield of the peptide sensor was measured using quinine sulfate (QY=0.427 in water) as the standard. The quantum yield was calculated as the follow equation:

$$\Phi_s = \Phi_r \frac{F_s}{F_r} \times \frac{A_r}{A_s}$$

Where Φs and Φr are the quantum yields of sample and the standard respectively; As and Ar are the respective absorbance of the sample and the standard; Fs and Fr are the areas of emission for sample and standard, respectively. The quantum yield was calcuiated to be 8.6%. The data of the lifetime were provided in Supporting Information Fig. S2 and Table S1.

3.2 Label-free and highly selective detection of Hg^{2+} ions with B,N-WS_2

RSC Advances Accepted Manuscript

To evaluate the selectivity of this sensing system, we examined the PL intensity changes in the presence of representative metal ions under identical conditions. Fig. 6 (a) shows the PL quenching results of B,N-WS_2 in the presence of Na^+, Al^{3+}, Ba^{2+}, Ca^{2+}, Cd^{2+}, Fe^{3+}, Fe^{2+}, Hg^{2+}, K^+, Li^+, Ag^+, Mg^{2+}, Cu^{2+}, Ni^{2+}, Pb^{2+} and Zn^{2+} (50 μM). As shown in Fig. 6 (a), evident PL quenching was observed upon the addition of Hg^{2+}. We found that among the tested ions only Ag^+ can quench the fluorescence of B,N-WS_2 nanosheets and may interfere with the Ag^+ detection. Fortunately, this issue can be circumvented by using Cl^- as chelating agents for Ag^+ ions and the results was shown in Supporting Information Fig. S3. The addition of Ag^+ ions into the B,N-WS_2 mixture in the presence of chelating agents has no effect on the detection of Hg^{2+}. Moreover, no tremendous decrease was observed by addition of these metal ions into the system.

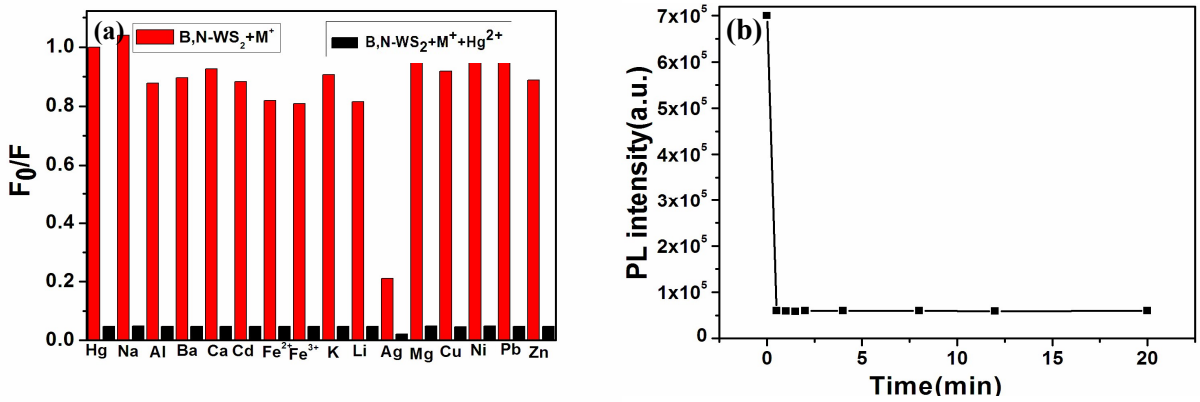

Fig. 6 Selective PL response of aqueous B,N-WS_2 solution toward different metal ions (excitation at 280 nm). F_0 and F are the fluorescence intensities of B,N-WS_2 at 343 nm in the absence and presence of metal ions (a). Fluoresence quenching of B,N-WS_2 by Hg^{2+} as a function of time (λ_{ex} = 280 nm) (b).

RSC Advances Accepted Manuscript

Fluorescence quenching kinetics was also studied. Fig. 6 (b) presents the time-dependent PL spectra of B,N-WS_2 dispersion after the addition of Hg^{2+}. Only 1 min was required to complete the reaction between B,N-WS_2 and Hg^{2+}, and no fluorescence change was observed within the following 12 h. All these observations indicate that the fluorescence of B,N-WS_2 was completely quenched within seconds upon adding Hg^{2+} and that detection is ultrafast.

Aside from selectivity, sensitivity is another important parameter in evaluating the performance of a sensing system. Therefore, the PL intensity changes with different concentrations of Hg^{2+} were studied to evaluate the sensitivity of the sensing system in this study. Fig. 7 shows the PL spectra of the B,N-WS_2 solution with different concentrations of Hg^{2+}. The result indicates that the PL intensity of the mixture is sensitive to Hg^{2+} concentration and decreases with the increase in Hg^{2+} concentration. The introduction of Hg^{2+} into the dispersion leads to significant decrease in fluorescence intensity, indicating that Hg^{2+} can effectively quench the fluorescence of B,N-WS_2 nanosheets. The interaction between Hg (soft donor) and sulfur atom (soft acceptor) is extremely strong[26,27]. Interaction is believed to be able to bring the atoms into close proximity. Given that the redox potential of Hg^{2+}/Hg^{+} lies between the conduction band (CB) and valence band (VB) of B,N-WS_2, photoinduced electron transfer from the CB to the complex Hg^{2+} occurs, leading to fluorescence quenching (Scheme 1).

RSC Advances Accepted Manuscript

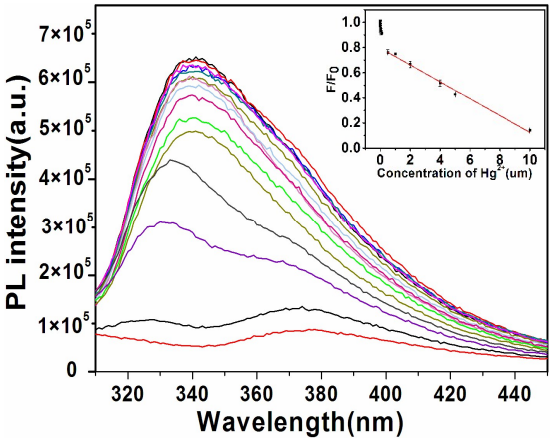

Fig. 7 PL spectra of B,N-WS_2 dispersion with different Hg^{2+} concentrations (From top to bottom: 0, 0.0005, 0.001, 0.0025, 0.002, 0.01, 0.02, 0.05, 0.1, 0.5, 1.0, 2.0, 4.0, 5.0, 8.0, and 10 μM of Hg^{2+}); Inset: dependence of F_0/F on the concentration of Hg^{2+} ions within the range of 0.0005–10 μM (F_0 and F are the B,N-WS_2 fluorescence intensities at 343 nm in the absence and presence of Hg^{2+} ions, respectively).

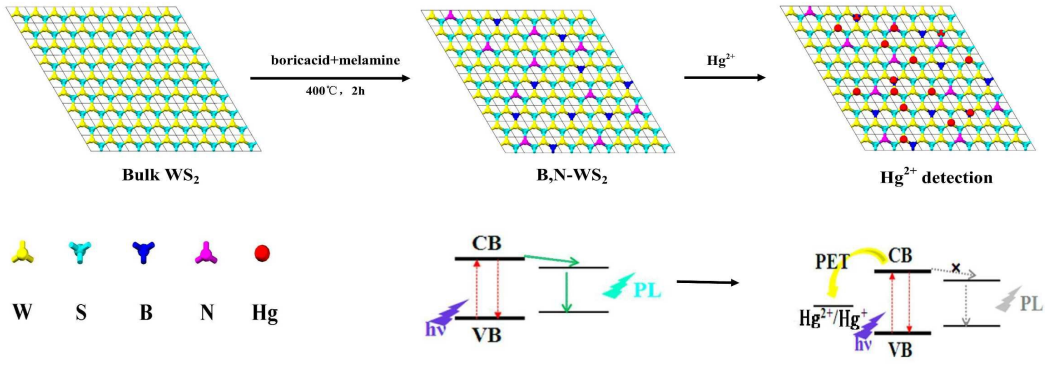

Scheme 1 Schematic of the sensing principle of the B,N-WS_2-based fluorosensor for Hg^{2+}.

The inset in Fig. 7 shows the dependence of F/F_0 on the concentration of Hg^{2+}. F_0 and F represent the fluorescence intensities of B,N-WS_2 at 343 nm in the absence and presence of Hg^{2+}, respectively. A good linear correlation was obtained over the

RSC Advances Accepted Manuscript

concentration range of 1 μM to 10 μM. The detection limit was estimated to be 23 nM at a signal-to-noise ratio (*S/N*) of 3. The detection limit has been compared to the other methods. Table S2 compares the sensing performance of different fluorescent probes for Hg^{2+}, showing that our sensing system exhibits superior sensitivity over previously reported sensing systems.

To demonstrate the practical use of the proposed, we performed a study to determine Hg^{2+} concentrations in tap water samples. As shown in Fig. 8, PL intensity decreases with increased concentration of Hg^{2+} from 0 μM to 0.4 μM. The calibration curve for determining Hg^{2+} in tap water was obtained by plotting the values of F_0/F-1 versus the concentrations of Hg^{2+} (Fig. 8, inset). The sensing system can distinguish between tap water spiked with 0.1 μM. In addition, the samples were also analyzed by cold vapor atomic absorption spectrometry (CV-AAS) as shown in table S3. The results suggest that the sensor is likely to be capable of practical Hg^{2+} detection upon further development. The proposed design is simple to prepare and exhibits low background interference, high sensitivity, and ultrafast response.

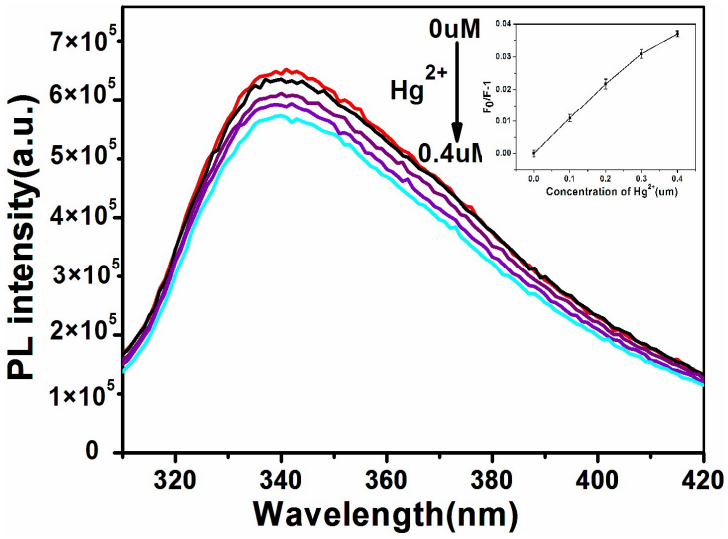

RSC Advances Accepted Manuscript

Fig. 8 PL spectra of B,N-WS_2 dispersion with different Hg^{2+} concentrations (From top to bottom: 0, 0.1, 0.2, 0.3, and 0.4 μM of Hg^{2+}); Inset: dependence of F_0/F-1 on the concentration of Hg^{2+} ions within the range of 0–0.4 μM (F_0 and F are the B,N-WS_2 fluorescence intensities at 343 nm in the absence and presence of Hg^{2+} ions, respectively).

4. Conclusions

We successfully developed a simple method for the preparation of B,N-doped WS_2 with boric acid and melamine as boron and nitrogen sources, respectively. The as-synthesized B,N-WS_2 exhibited enhanced fluorescence in comparison with undoped WS_2 and utilized as a highly efficient fluorescence sensor for selective detection of Hg^{2+}. The detection is rapid and ultrasensitive, with an extremely low detection limit of 23 nM (S/N = 3). The present study is important because it demonstrates an economic, stable, and environment-friendly route toward the production of B,N-WS_2 for rapid, highly selective, and sensitive optical detection of Hg^{2+} for the first time. This method may open up a potential approach for designing more efficient TMD-based biosensors and fluorescence materials.

Acknowledgements

This work is supported by National Natural Science Foundation of China (31270988, 31401577), National Undergraduate Innovational Experimentation Program (201310530007), Scientific Research Fund of Hunan Provincial Education

RSC Advances Accepted Manuscript

Department (13B120), China Postdoctoral Science Foundation (2014M562118) and Hunan Provincial Natural Science Foundation of China (2015JJ2133, 13JJ9004).

References

1 M. B. Gumpu, S. Sethuraman, U. M. Krishnan and J. B. B. Rayappan, *Sens. Actuators B*, 2015, **213**, 515-533.

2 S. Ando and K. Koide, *J. Am. Chem. Soc.*, 2011, **133**, 2556-2566.

3 J. Gutknecht, *J. Membrane Biol.*, 1981, **61**, 61-66.

4 H. Huang, J. J. Lv, D. L. Zhou, N. Bao, Y. Xu, A. J. Wang and J. J. Feng, *RSC Adv.*, 2013, **3**, 21691-21696.

5 A. N. Liang, L. Wang, H. Q. Chen, B. B. Qian, B. Ling and. J. Fu, *Talanta*, 2010, **81**, 438-443.

6 Y. M. Guo, Z. Wang, H. W. Shao and X. Y. Jiang, *Carbon*, 2013, **52**, 583-589.

7 Y. R. Zhu, H. Li, B. B. Shi, W. J. Qu, Y. M. Zhang, Q. Lin, H. Yao and T. B. Wei, *RSC. Adv*., 2014, **4**, 61320-61323.

8 J. Hou, J. Li, J. Sun, S. Ai and M. Wang, *RSC. Adv.*, 2014, **4**, 37342-37348.

9 D. Zhang, M. Wang, C. C. Wang, M. Li, Y. Ye and Y. F. Zhao, *J. Fluoresc.*, 2013, **23**, 1045-1052.

10 Y. H. Lin and. W. L. Tseng, *Anal. Chem.*, 2010, **82**, 9194-9200.

11 L. Zhou, Y. Lin, Z. Huang, J. Ren and X. Qu, *Chem. Commun.,* 2012, **48**, 1147-1149.

12 J. Xie, H. Zhang, S. Li, R. Wang, X. Sun, M. Zhou, J. Zhou, X. W. Lou and Y. Xie, *Adv. Mater.*, 2013, **25**, 5807-5813.

RSC Advances Accepted Manuscript

13 X. Xu, C. S. Rout, J. Yang, R. Cao, P. Oh, H. S. Shin and J. Cho, *J. Mater. Chem. A*, 2013, **1**, 14548-14554.

14 D. Jariwala, V. K. Sangwan, L. J. Lauhon, T. J. Marks and M. C. Hersam, *ACS Nano*, 2014, **8**, 1102-1120.

15 D. J. Li, U. N. Maiti, J. Lim, D. S. Choi, W. J. Lee, Y. Oh, G. Y. Lee and S. O. Kim, *Nano Lett.*, 2014, **14**, 1228-1233.

16 A. K. Geim and I. V. Grigorieva, *Nature*, 2013, **499**, 419-425.

17 M. Xu, T. Liang, M. Shi and H. Chen, *Chem. Rev.*, 2013, **113**, 3766-3798.

18 M. Chhowalla, H. S. Shin, G. Eda, L. J. Li, K. P. Loh and H. Zhang, *Nat. Chem.*, 2013, **5**, 263-275.

19 M. Pumera and A. H. Loo, *TrAC Trends Anal. Chem.*, 2014, **61**, 49-53.

20 X. Yang, J. Li, T. Liang, C. Ma, Y. Zhang, H. Chen, N. Hanagata, H. Su and M. Xu, *Nanoscale*, 2014, **6**, 10126-10133.

21 A. Jäger-Waldau, M. C. Lux-Steiner, G. Jäger-Waldau and E. Bucher, *Appl. Sur. Sci.,* 1993, **70**, 731-736.

22 Y. Zhou, J. Dong and H. Li, *RSC. Adv.*, 2015, **5**, 66852-66860.

23 G. Kline, K. Kam, D. Canfield and B. A. Parkinson, *Sol. Energy Mater.*, 1981, **4**, 301-308.

24 P. C. Yen, H. P. Hsu, Y. T. Liu, Y. S. Huang and K. K. Tiong, *J. Physics: Conden. Matter*, 2004, **16**, 6995-7005.

25 P. C. Yen, Y. S. Huang and K. K. Tiong, *J. Physics: Conden. Matter*, 2004, **16**, 2171-2180.

RSC Advances Accepted Manuscript

26 Y. Guo, L. Zhang, S. Zhang, Y. Yang, X. Chen and M. Zhang, *Biosens. Bioelectron.*, 2015, **63**, 61-71.

27 H. Gonçalves, P. A. S. Jorge, J. R. A. Fernandes and J. C. G. Esteves da Silva, *Sens. Actuators B*, 2010, **145**, 702-707.

28 R. Freeman, T. Finder and I. Willner, *Angew. Chem. Int. Ed.*, 2009, **48**, 7818-7821.

29 R. Zhang and W. Chen, *Biosens. Bioelectron.*, 2014, **55**, 83-90.

30 B. Paramanik, S. Bhattacharyya and A. Patra, *Chem. Eur. J.*, 2013, **19**, 5980-5987.

31 S. J. He, B. Song, D. Li, C. F. Zhu, W. P. Qi, Y. Q. Wen, L. H. Wang, S. P. Song, H. P. Fang and C. H. Fan, *Adv. Funct. Mater.*, 2010, **20**, 453-459.

32 X. Wang, P. Wang, Z. Dong, Z. Dong, Z. Ma, J. Jiang, R. Li and J. Ma, *Nanoscale Res. Lett.*, 2010, **5**, 1468-1473.

33 N. Y. Fu, Y. Q. Chen, J. Fan, G. M. Wang and S. Y. Lin, *Sens. Actuators B*, 2014, **203**, 435-443.

34 Y. P. Zhu, T. Y. Ma, T. Z. Ren and Z. Y. Yuan, *ACS Appl. Mater. Interfaces.*, 2014, **6**, 16344-16351.

35 H. S. So, B. A. Rao, J. Hwang, K. Yesudas and Y. A. Son, *Sens. Actuators B*, 2014, **202**, 779-787.

RSC Advances Accepted Manuscript